THE INNER BREMSSTRAHLUNG SPECTRUM OF Co^{57}

by

JERRY D. GANN, B. S.

A THESIS

IN

PHYSICS

Submitted to the Graduate Faculty
of Texas Technological College
in Partial Fulfillment of
the Requirements for
the Degree of

MASTER OF SCIENCE

May, 1962

TABLE OF CONTENTS

LIST OF ILLUSTRATIONS

Figure

CHAPTER I

INTRODUCTION

When a nucleus decays by orbital electron capture, the disintegration energy can be shared by a photon and a neutrino. This electromagnetic radiation, which accompanies some of the disintegrations and is called inner Bremsstrahlung, has a continuous energy distribution. This distribution in energy ranges from zero to an upper limit which is the disintegration energy minus the binding energy of the captured electron. Morrison and Schiff (1) made an effort to predict the intensity of this energy spectrum by considering only electron capture from the 1S state. More recently Glauber and Martin (2, 3) have developed an expression for the predicted intensity by considering capture from the different electron states as well as relativistic and screening effects.

The purpose of this thesis is to determine experimentally the absolute intensity of the inner Bremsstrahlung spectrum of Co^{57} as a function of energy and to compare it with the prediction of Glauber and Martin. After the corrections due to crystal effects have been applied to the theoretical spectrum, it will then be compared with the experimentally observed spectrum.

CHAPTER II

THEORY

General Discussion

The decay of a nucleus by orbital electron capture results in the creation of a neutron inside the nucleus and the annihilation of a proton and the captured electron. The emission product ordinarily is a neutrino which has a discrete energy equal to the disintegration energy minus the binding energy of the captured electron. An event of much rarer occurence results in the simultaneous emission of a neutrino and a photon, inner Bremsstrahlung, both having a continuous range of energy values available (4).

An electron may be captured from any of the atomic electron states. The probability of capture from any state is determined by the square of the absolute value of the corresponding wave function evaluated at the nuclear origin. The wave function for 1S electrons is usually the largest at the origin with the wave functions of the 2S, 2P, and 3P states being somewhat smaller. The possibility of capture from states above the 3P is not considered in the development of the theory since the capture probability is so small.

The Morrison and Schiff Theory

Morrison and Schiff (1) made an effort to predict the variation in intensity of the inner Bremsstrahlung, hereafter designated as IB, with energy by considering only electron capture from the 1S state. For allowed transitions, the IB spectrum has the shape of the form $x\,(1-x)^2$, where x is the ratio of K, the energy of a given photon, to W, the disintegration energy minus the binding energy of the 1S state. The ratio of ω_{1s}, the probability of radiative capture from the 1S state with the IB energy K in the energy interval dK, to ω_K, the capture probability of 1S electrons, is given by

$$\frac{\omega_{1s}}{\omega_K}\,dK = \frac{\alpha}{\pi}\left(\frac{W}{m}\right)^2 \left[1 - \frac{K}{W}\right]^2 \frac{K}{W}\,d\,\frac{K}{W} \quad .$$

In the above equation, α is the hyperfine constant, and m is the rest energy of the electron. Integration of this equation over the range of K/W of 0 to 1 yields

$$\int_0^W \frac{\omega_{1s}}{\omega_K}\,dK = \frac{\alpha}{12\pi}\left(\frac{W}{m}\right)^2 \quad .$$

The predicted shape of the spectrum compares favorably with experimentally observed spectra except in the low energy region where there is an unpredicted increase in intensity.

The Glauber and Martin Theory

Glauber and Martin (2, 3) have developed a much more complete theory by considering electron capture from the 1S, 2S, 2P, and 3P states as well as relativistic and screening effects. The theory is based on the fact that the electron radiates the photon, IB, during a virtual transition to an intermediate state from which it is captured by the nucleus. Only spherically symmetric wave functions differ from zero at the nucleus so the intermediate state is an S state. Although the exclusion principal requires that no virtual transition can be made to an occupied S state, it can be shown that equal transition amplitudes occur from processes in which the obstructing electron is captured before radiative emission.

The radiation resulting from capture from an initially occupied S state involves a reorientation of the electron spin since a spinless particle cannot emit a photon during a transition. Radiative capture from the P state takes place when the electrons make an electric dipole transition to an intermediate S state from which they are captured by the nucleus. The continuous spectrum resulting from capture from the P state is very intense in the region of the characteristic x-ray.

The relativistic correction is quite large since it involves primarily the relativistic electron spin. Three

processes, open to electrons in the S state, are treated in the theory; the reorientation of the electron spin during radiative capture; the emission of a single quantum when a virtual positron, ejected by the nucleus, annihilates an electron; and the transition of S state electrons to $P_{\frac{1}{2}}$ states from which capture takes place. Atomic screening has little effect on capture from the 1S state since it is so close to the nucleus, but screening causes a very significant reduction in capture from the 2S, 2P, and 3P states which are farther from the nucleus. Neither the relativistic correction nor the screening corrections appreciably alter the shape of the IB spectrum.

If one considers capture from these four states only, the ratio of the probability of radiative capture from the $n\ell$ shell with the emitted IB of energy K, $\omega_{n\ell}(K)$, to the capture probability of 1S electrons, ω_K, is

$$\frac{\omega_{n\ell}(K)}{\omega_K}\, dK = \frac{\alpha}{\pi}\left(\frac{1}{2} Z^2 \alpha^2\right) I_{n\ell}(K) \left[\frac{W - (K + \epsilon_{n\ell} - \epsilon_{1s})}{W}\right]^2 \frac{S_{n\ell}}{S_{1s}}\, dK$$

where K is measured in units of the 1S binding energy, $(Z\alpha)^2\, m/2$. The constants $\epsilon_{n\ell}$ and ϵ_{1s} are the positive

binding energies of the $n\ell$ electron shells. The screening correction, $S_{n\ell}$, is the ratio of the screened wave function to the unscreened wave function evaluated near the origin. A graph of values for $S_{n\ell}$, reproduced from an unpublished report by Brysk and Rose (5), is given in the second paper by Glauber and Martin (3). The intensity function $I_{n\ell}(K)$ has the two forms

$$I_{ns} = K\, R_{ns}(K) \left[\frac{\phi_{ns}(0)}{\phi_{1s}(0)} \right]^2$$

and

$$I_{np} = \left(\frac{2}{Z\alpha} \right)^2 \left[Q_{np}(K) \right]^2 .$$

The two quantities $R_{ns}(K)$ and $Q_{np}(K)$, both functions of energy, are the relativistic correction factor and the value of the integral used in calculating the P-state spectra, respectively. Values of $Q_{np}(K)$ are given numerically for $n = 2$ and $n = 3$ in the first paper by Glauber and Martin (2). $\Phi_{ns}(0)$ and $\Phi_{1s}(0)$ are the values of the wave functions of the ns and 1S states near the origin. Values of the wave functions were taken from the unpublished report by Brysk and Rose (5). The constant Z is the nuclear charge. For the 1S state, the above relation reduces to the Morrison-Schiff relation if no relativistic correction is made; that is, $R_{1s} = 1$.

For the 1S state, the relativistic correction takes the form

$$R_{1s} = \frac{1}{2} (A_{1s}^2 + B_{1s}^2)$$

where

$$A_{1s} = 1 - Z\alpha \left\{ \left(\frac{\mu}{K} \right) + 2 \left[1 - \frac{m}{K} \right] \tan^{-1} \left(\frac{K}{\mu} \right) \right\}$$

and

$$B_{1s} = 1 - Z\alpha \left\{ \left(\frac{\mu}{K} \right) \left[1 \ \frac{m}{K} \right] + 2 \left[1 - \left(\frac{m}{K} \right)^2 \right] \right.$$

$$\left. \tan^{-1} \left(\frac{K}{\mu} \right) \right\} .$$

The quantity μ is given by

$$\mu = \left[m^2 - (\epsilon_{1s} - K)^2 \right]^{\frac{1}{2}}$$

with $\epsilon_{1s} = m \left[1 - (Z\alpha)^2 \right]^{\frac{1}{2}}$.

As K approaches zero, a better approximation for A_{1s} and B_{1s} can be expressed as

$$A_{1s} = \frac{1}{2} (2\lambda + 1) \left[1 - \frac{K}{m} \right]$$

and

$$B_{1s} = 0 + 0 \left(\frac{K}{Z\alpha m} \right)$$

levels

where $\lambda = \left[1 - (Z\alpha)^2\right]^{\frac{1}{2}}$. A plot of $R_{1s}(K)$ for Co^{57} is given in Figure 1. The relativistic correction used in the calculations for the 2S state is given numerically in the first paper by Glauder and Martin (2).

Approach to the Problem

There are several advantages in using Co^{57} to study an IB spectrum. Since the element decays by orbital electron capture, there is no external Bremsstrahlung accompanying the emission of charged particles to mask the rather weak IB. Also, the K-shell x-rays do not interfere because of their low energy of 6.4 kev. As the disintegration energy of Co^{57} is about 430 kev, the IB spectrum covers a considerable energy range. One difficulty that arises is caused by the presence of the gamma radiation emitted in the decay from the excited levels of Fe^{57}. The decay of Co^{57} is given in Figure 2.

Because of the gamma emission from the excited levels of Fe^{57} in the decay of Co^{57}, coincidence techniques were used to eliminate the 122 kev and 136 kev gamma rays from the IB spectrum. This results in a continuous IB spectrum composed of contributions characteristic of all electron levels. Since the probability of capture from any level greater than 3P is extremely small, the work of Gauber and Martin considered only capture from the four lower levels. The final theoretical equation takes the form

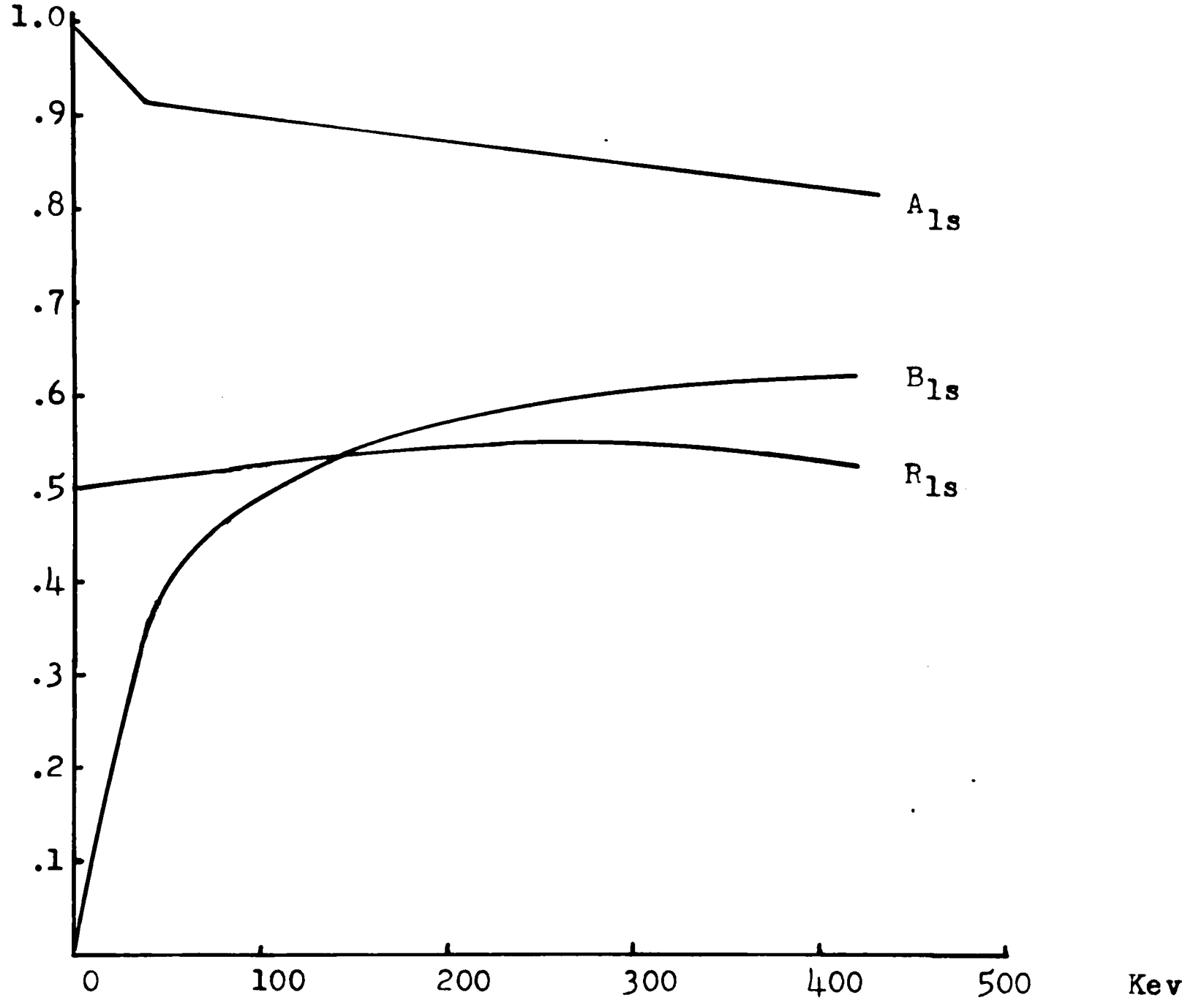

Figure 1. Relativistic Correction Factor for the 1S State

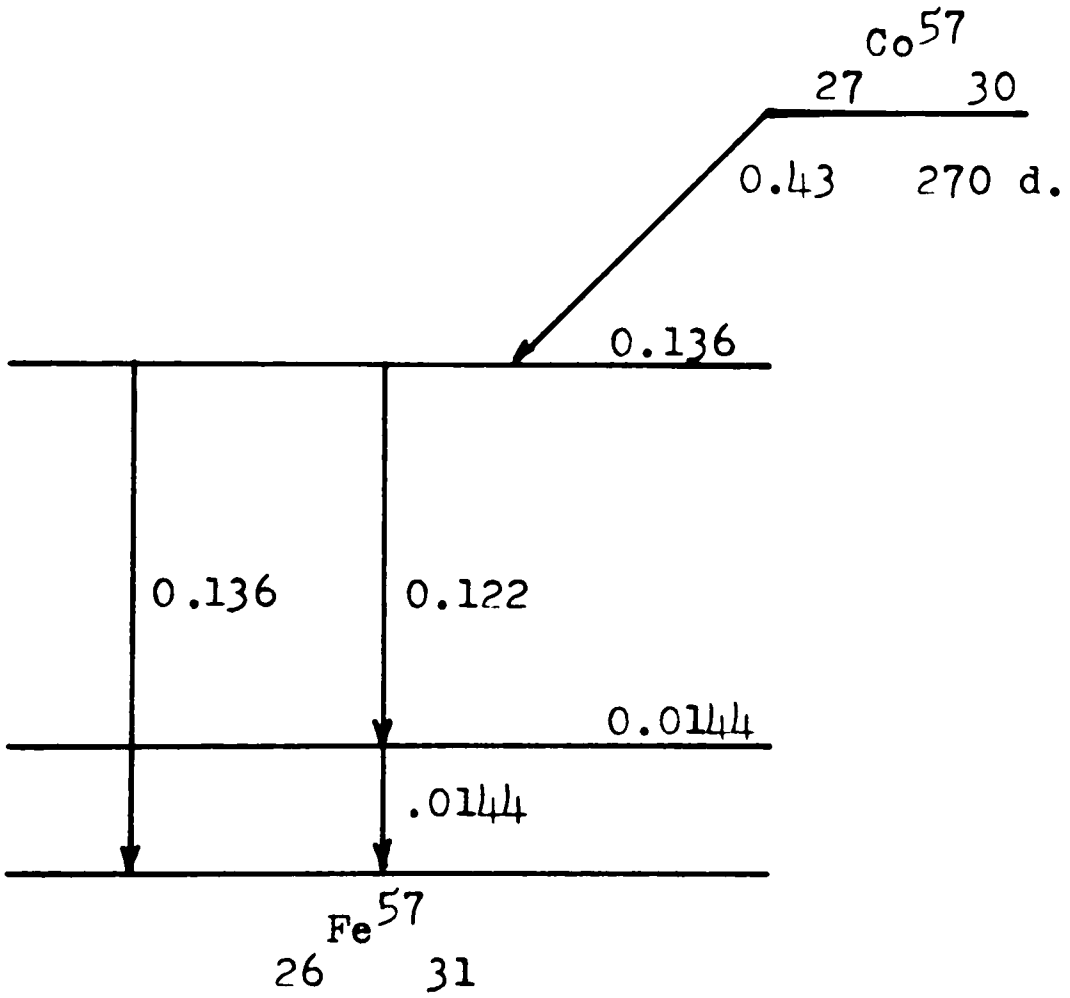

Figure 2. Decay Scheme of Co^{57}

$$\frac{\omega_{IB}(K)}{\omega_K}\,dK = \left[\frac{\omega_{1s}(K)}{\omega_K} + \frac{\omega_{2s}(K)}{\omega_K} + \frac{\omega_{2p}(K)}{\omega_K} + \frac{\omega_{3p}(K)}{\omega_K}\right] dK$$

where $\omega_{IB}(K)/\omega_K$ is the ratio of the probability of IB emission of energy K in the energy interval dK to the probability of K capture. The total theoretical IB spectrum of Co^{57} is given in Figure 3.

Since radiative capture from the 1S state is the main contribution to the IB spectrum, one can get some indication as to the difficulty involved in this coincidence experiment by making use of the Morrison and Schiff equation

$$\int_0^W \frac{\omega_{1s}(K)}{\omega_K}\,dK = \frac{\alpha}{12\pi}\left(\frac{W}{m}\right)^2 .$$

If one assigns W = 430 kev, this equation yields a value of 1.31 10^{-4} as the ratio of the probability of radiative capture from the 1S state to the probability of 1S capture. The Glauber and Martin theory predicts that this figure will be reduced even further by the relativistic correction.

The number of IB in the energy interval dK in coincidence with either the 122 kev or 136 kev gamma ray per unit time, $N^{(K)}_{IB-122+136}$, can be found from the coincidence equation

$$N^{(K)}_{IB-122-136}\,dK = N_0\left[\frac{\omega_{IB}(K)}{\omega_0}\,dK\right]\epsilon_{IB}(K)\,P_{122+136} .$$

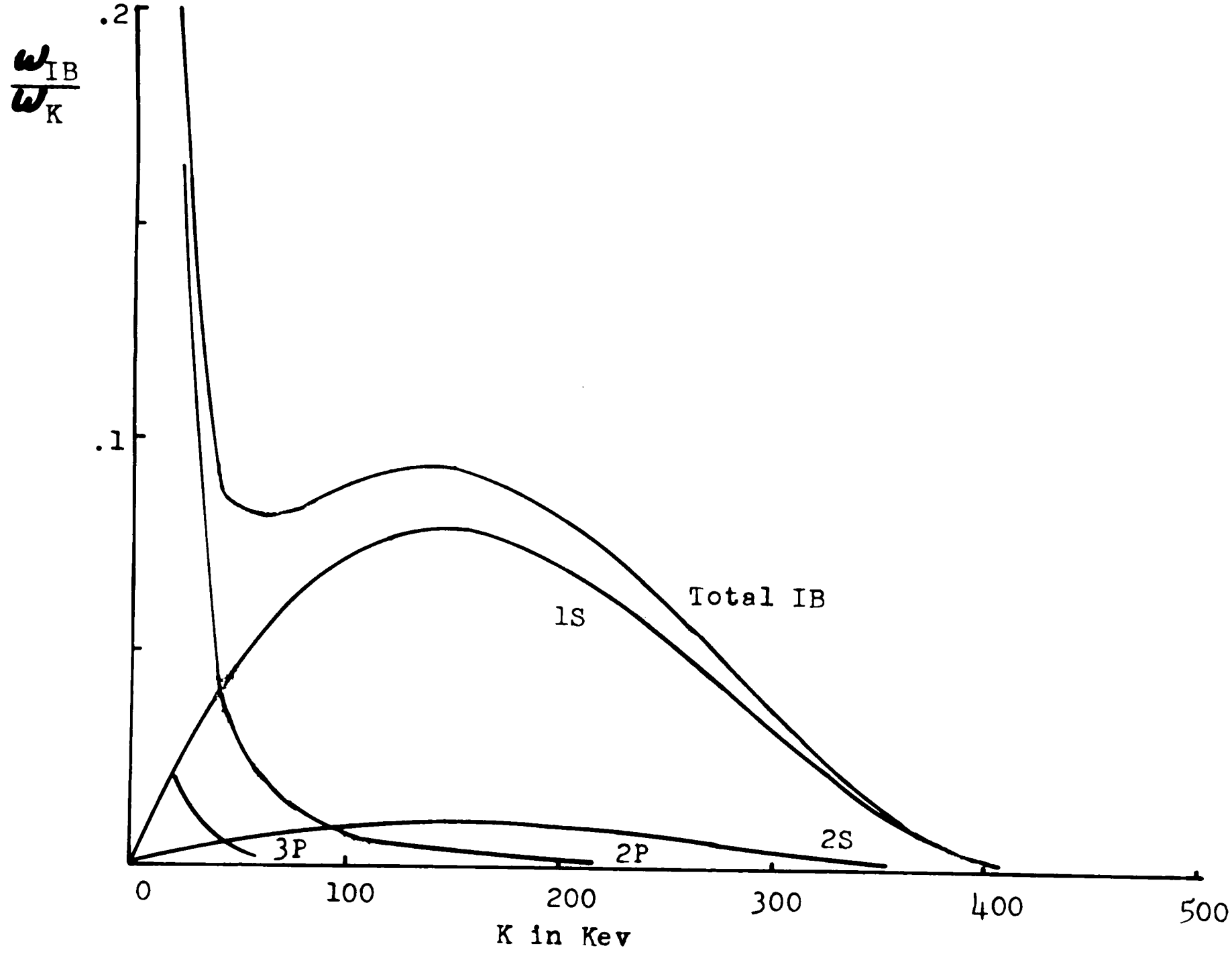

Figure 3. Theoretical IB Spectrum of Co^{57}

In the above equation, N_0 is the disintegration rate; $\left[\frac{\omega_{IB(K)}}{\omega_0} dK\right]$ is the ratio of the probability of IB emission in the energy interval dK to the probability of electron capture; $\epsilon_{IB}(K)$ is the absolute efficiency of the detector for the IB; and $P_{122+136}$ is the probability that a 122 kev or 136 kev gamma ray will be detected and the corresponding pulse will pass through the window in the gating circuit. The single channel count rate, $N_{122+136}$, can be expressed as

$$N_{122+136} = N_0 P_{122+136} .$$

The quantity $P_{122+136}$ has the form

$$P_{122+136} = \left\{ p \left(\frac{1}{1+\alpha_{122}} \right) \epsilon_{122} f_{122} + (1-p) \left(\frac{1}{1+\alpha_{136}} \right) \epsilon_{136} f_{136} \right\} .$$

The total internal conversion coefficients for the 122 kev and 136 kev transitions are given by α_{122} and α_{136}, respectively; p is the ratio of the number of 122 kev transitions to N_0; ϵ_{122} and ϵ_{136} are the absolute efficiency of the detector for the 122 kev and 136 kev gamma rays, respectively; and f_{122} and f_{136} represent the fraction of the 122 kev and 136 kev gamma ray pulses, respectively, which pass through the window in the gating circuit.

The quantity $P_{122+136}$ is a constant which will not vary during the experiment.

If $N_{IB-122+136}(K)\,dK$ is divided by $N_{122+136}$, the resulting expression is

$$\frac{N_{IB-122+136}(K)\,dK}{N_{122+136}} = \left(\frac{\omega_{IB}(K)}{\omega_c}\right)\epsilon_{IB}(K)\,dK \quad .$$

The probability of capture, ω_c, can be expressed as the sum of the probabilities of capture from all electron states $\omega'_{n\ell}$,

$$\omega_c = \omega'_{1s} + \omega'_{2s} + \omega'_{2p} + \omega'_{3p} + \cdots \quad .$$

By factoring out ω'_{1s}, one obtains

$$\omega_c = \omega'_{1s}\left[1 + \frac{1}{\omega'_{1s}}\left(\omega'_{2s} + \omega'_{2p} + \omega'_{3p} + \cdots\right)\right] .$$

By defining ϵ_K as the ratio of the sum of the probabilities of capture from all electron states except the 1S state to the probability of capture from the 1S state, one obtains

$$\omega_c = \omega'_{1s}\left[1 + \epsilon_K\right]$$

or, since $\omega'_{1s} = \omega_K$,

$$\omega_c = \omega_K\,(1 + \epsilon_K) \quad .$$

The coincidence equation now becomes

$$\frac{N_{IB-122+136}^{(K)}}{N_{122+136}} \, dK \, (1+\epsilon_K) = \left(\frac{\omega_{IB}^{(K)}}{\omega_K}\right) \epsilon_{IB}(K) \, dK \quad .$$

The right side of the above equation contains the theoretical results corrected for detection efficiency, and the left side contains the experimental results. An absolute intensity measurement may be made by recording $N_{122+136}$ and by making use of ϵ_K. The value of ϵ_K was determined to be very close to 0.1 from the tables of Wapstra, Nijgh, and Lieshout (6).

CHAPTER III

METHODS AND PROCEDURES

Preparation of the Source

The source was prepared by electroplating Co^{57} from a solution of cobalt chloride in hydrochloric acid onto an aluminum foil 0.02 millimeters thick. Abbott Laboratories supplied the solution which on July 26, 1960 had a specific activity of 6600 mc/mg.

A few drops of plating solution were placed in a tapered hole drilled through a one-half inch thick lucite block which acted as an insulator. The aluminum foil was placed between the lucite block and a piece of aluminum stock so that it formed one electrode. The other electrode consisted of an adjustable screw, the supports of which were placed on top of the lucite in such a way that it could be lowered into the hole.

The foil was first cleaned with acetone and then treated with a sodium hydroxide solution. Concentrated nitric acid was used to remove any contaminants which might be present. The foil was then washed with distilled water.

Since cobalt will not deposit directly on aluminum, the surface was anodized. After the surface was washed,

a 75% phosphoric acid solution was brought in contact with the surface and a current of 10 milliamperes was passed through the solution for 10 minutes. The surface was then washed with distilled water.

The plating solution (7) consisted of:

Rochelle salt	400 g/l.
Ammonium chloride	50 g/l.
Ammonium hydroxide to pH	8.5
Temperature 90° C. or above	

The radioactive Co^{57} was deposited inside a circle about 3 millimeters in diameter. For the first thirty seconds, the current was held at 8 milliamperes and then decreased to 4 milliamperes for the duration of the run, 25 minutes. The coated surface was then washed several times with distilled water.

Description of Equipment

The presence of the discrete gamma radiation from the excited levels of Fe^{57} in the decay of Co^{57} necessitated the use of coincidence techniques to remove them from the IB spectrum. The purpose of the coincidence system is to activate the multichannel analyzer when an IB and a 122 kev or 136 kev gamma ray are detected in coincidence. The multichannel analyzer then analyzes the pulses according to amplitude, which is proportional to the energy of the detected radiation. The multichannel analyzer was a Radiation Counter Laboratory, Model 20609, 256-channel analyzer.

Two scintillation detectors were used; both consisted of 2" x 2" sodium iodide, thallium activated, crystals which were mounted in this laboratory on Dumont 6292 photomultiplier tubes and covered with 10 mil beryllium sheets.

The block diagram of the equipment used is given in Figure 4. The two detectors, D-1 and D-2, were placed facing each other. The source was placed 0.8 cm from D-1 and 1.4 cm from D-2. Each detector was connected to a pre-amplifier, P. A., which in turn was connected to a linear amplifier, L. A., and to a differential pulse height analyzer. One differential pulse height analyzer, D.P.A.-2, was gated so that only 122 kev or 136 kev pulses were passed while the other, D.P.A.-1, was gated just above the noise level. The gate of D.P.A.-2 was set so that it did not include the escape peak corresponding to the 122+136 kev peak. L. A.-1 was a Hamner Electronic Co., Model N302, Non-Overload Amplifier, and L. A.-2 was a Franklin Electronic, Model 348, Linear Amplifier.

The outputs of both D.P.A.-1 and D.P.A.-2 were fed to a slow coincidence input; the outputs of L. A.-1 and L. A.-2 were fed to a fast coincidence input. The coincidence circuit, C. C., was a Detectolab, Model DZ4, Coincidence Circuit. The D.P.A. units delay a pulse about 1.5μs. and have a 0.5μs uncertainity in the time needed to analyze the pulse. Since a linear amplifier does not have this uncertainity, the L. A. outputs are connected to

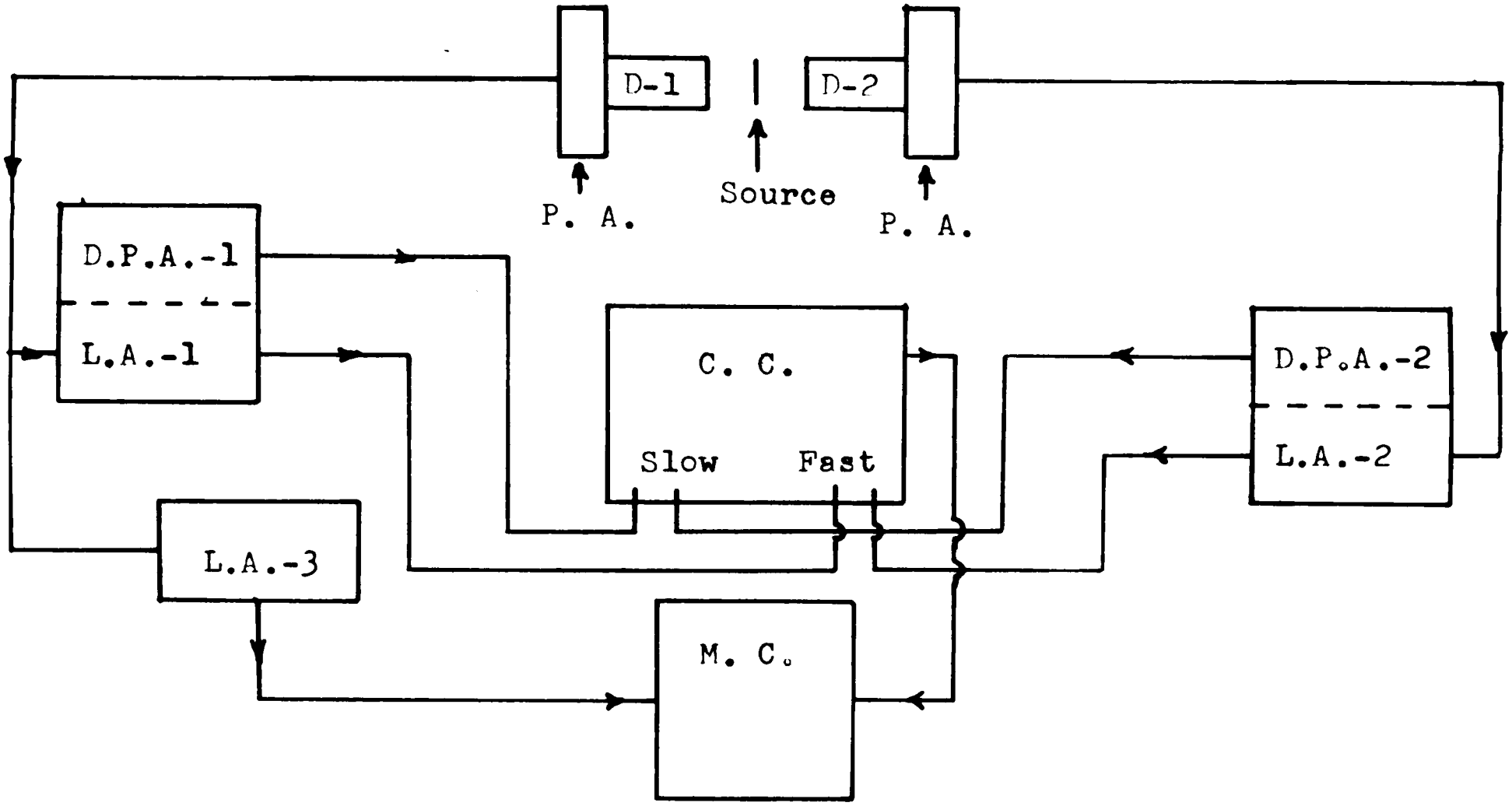

Figure 4. Block Diagram of Equipment

the fast element. Therefore the coincident pulses from L. A.-1 and L. A.-2 arrive at the fast inputs at the same time; the pulses arrive at the slow inputs 1.5μs later. A delay line with a time delay of 1.5μs was inserted in the fast element of the coincidence circuit to bring the timing of the slow and fast elements together. The two slow elements and the fast element are fed to a triple slow coincidence element.

D-1 is connected to the multichannel analyzer, M. C., through the A-61 Linear Amplifier, L. A.-3, included in the multichannel analyzer. A delay line with a time delay of 1.5μs is included in the M. C. unit so that a pulse from D-1 will arrive at the same time as a pulse from the C. C. unit.

In order to obtain the IB spectrum, the random coincidence must be subtracted from the true coincidences. The random coincidence curve was obtained with a delay line between D-2 and L. A.-2 so that one of the slow inputs and one of the fast inputs were delayed 3μ sec.

It was found that the coincidence rate caused by the background was significant. This was obtained by removing the source and running for the same length of time as with the source.

CHAPTER IV

DATA AND ANALYSIS

Analysis of the Theoretical Spectrum

A comparison of the theoretical spectrum with the experimental spectrum can be made only after the corrections due to crystal effects have been applied. The corrections for efficiency and absorption are the first to be made. A 353 mg/cm^2 aluminum absorber was placed over the scintillation counter to remove the 14.4 kev gamma radiation from the IB spectrum. Each ordinate of the theoretical IB spectrum was multiplied by the absolute detection efficiency and by the fraction of radiation transmitted by the absorber. Both the absolute efficiency and the absorption are a function of energy. The absolute detection efficiency for a 2" x 2" sodium iodide crystal is given by R. L. Heath (8). The absolute detection efficiency curve, $\epsilon(K)$, for the geometry used is reproduced in Figure 5. When this correction is applied, the resulting curve represents the detected IB spectrum.

Once a gamma ray enters the crystal, it may or may not be recorded at full energy. If it causes the ejection of a photoelectron, it will be recorded with the full energy; but if the gamma ray is Compton scattered, it may be

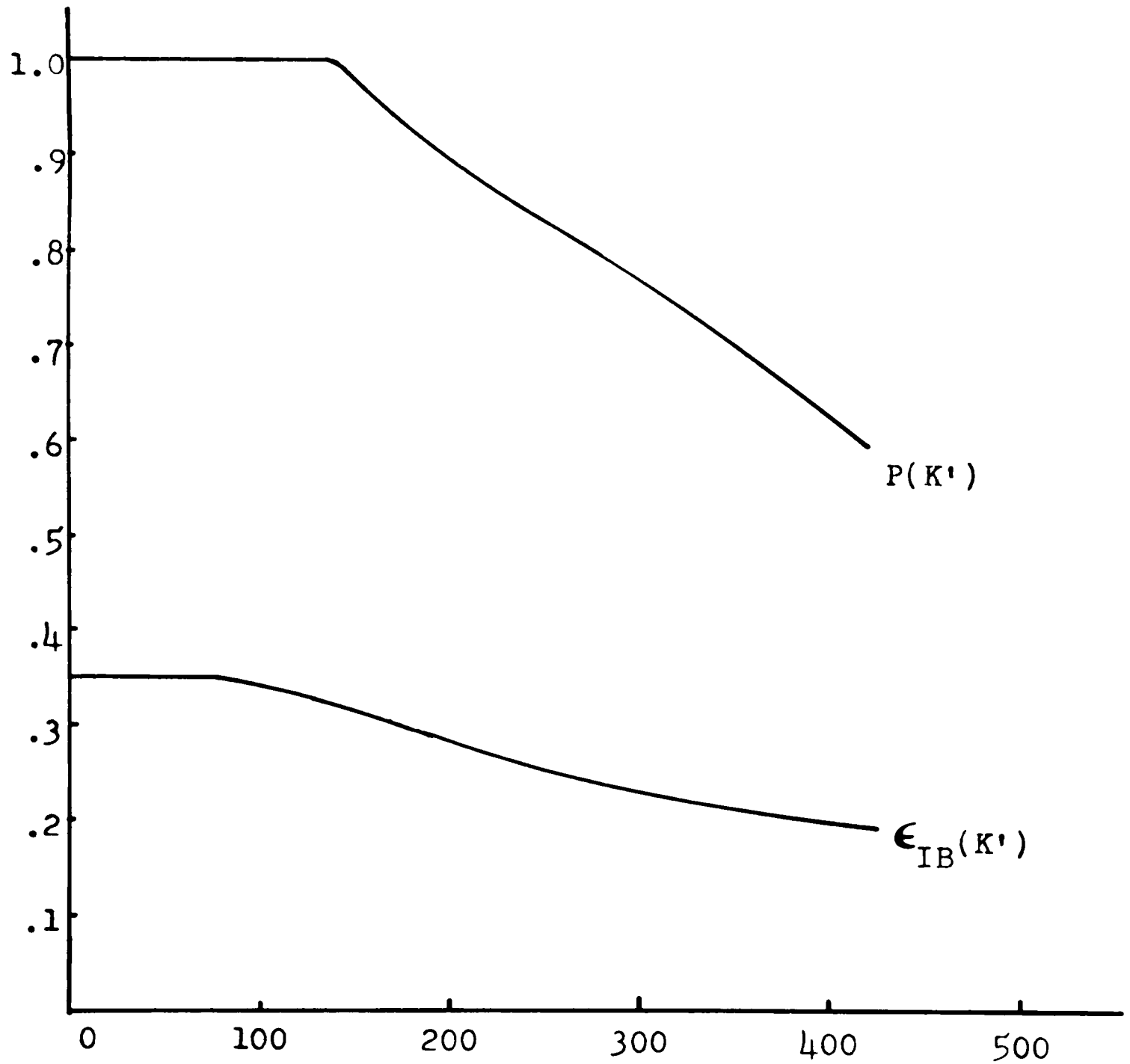

Figure 5. Values of P(K') and $\epsilon_{IB}(K')$

recorded with less than full energy. The fraction, p(K'), of the detected radiation which will be recorded as having the full energy can be determined experimentally. This is accomplished by obtaining a spectrum of a source which emits gamma radiation of only one energy and then determining the ratio of the area under the photopeak to the total area under the spectrum. This procedure must be repeated for several different sources over a considerable energy range since p(K') is energy dependent. To determine the ordinate, $I_p(K')$, of the IB detected at full energy, each ordinate of the detected IB spectrum is multiplied by the corresponding ratio, p(K').

For this experiment, a spectrum of Sn^{113} was run giving a value of 0.64 for p(K') at 392 kev. This value of p(K') was used to normalize a curve of p(K') given for a 3" x 3" sodium iodide crystal by R. L. Heath (8), thus resulting in a different curve having new ordinate values but with the same slope. The curve for p(K') is given in Figure 5.

The procedure following in correcting for the Compton scattered gamma radiation is given in an article by Lindquist and Wu (9). The fraction of photons recorded with less than full energy is given by $\left[1-p(K')\right]$; K' designates the IB energy. Therefore, the total number of Compton scattered electrons is given by $I_p(K')\left[1-p(K')\right]$, for any specific I_p. These electrons have an energy range from K = 0 to $K = K^*$, where K^* is the maximum Compton electron energy

corresponding to K'. The probability that a Compton electron will lie in the energy interval K to K+dK is given by C (K, K') which is approximately constant over a range K = 0 to K = K*. This function can be expressed as

$$C\ (K,\ K') = C\ (K') = \frac{1}{K^*}\ ,\ 0 < K < K^*$$

$$C\ (K,\ K') = 0\ ,\ K > K^*\ .$$

To obtain the Compton distribution, one must perform a step by step integration. The ordinate of the Compton distribution, with the energy of the electrons ranging from K = K*, for photons with an energy between K' and K'+ΔK' is given by

$$\Delta I_c = \frac{1}{K^*}\ I_p(K')\ \left[1 - p(K')\right]\Delta K'\ .$$

The Compton distribution can be found by adding all the various values ΔI_c computed for each $I_p(K')$.

When a photoelectron is ejected from an atom, it has an energy corresponding to the energy of the photon minus the binding energy of the electron shell from which it came. As the vacant electron shell is filled, either an Auger electron or an x-ray can be emitted. If the Auger electron is emitted, the energy of the photon is recorded with the full value. When the x-ray escapes from the crystal, the energy of the photon is recorded as the initial energy minus the binding energy of the electron shell. For K x-ray escape, this effect is important only at low energies,

$K' \lesssim 150$ kev. The ratio of the number of K x-rays that escape from a sodium iodide crystal to the number of incident gamma rays normal to the surface, $P_E(K')$, has been calculated for a semi-infinite crystal. The values were used in correcting for the K x-ray escape. The ordinate of the escape curve, $I_E(K)$, was obtained by multiplying $I_p(K')$ by the corresponding ratio $P_E(K')$. The escape curve is constructed by plotting the values of $I_E(K)$ at $K = K' - 28$ kev. The altered values of $I_p(K')$, $I'_p(K')$, is found by subtracting $I_E(K)$ from $I_p(K')$. For values of $K' > 150$ kev, $I'_p(K')$ is equal to $I_p(K')$.

The ordinate of the resulting curve, $I_T(K')$ is obtained by adding the ordinates of all three curves at each value of K', $I_T(K') = I_E(K') + I_c(K') + I'_p(K')$. This curve is given in Figure 6.

The ratio of the area under the backscattered peak to the area under the photopeak obtained from the Sn^{113} spectrum was 0.066. No correction for backscattering was applied to the theoretical distribution. This curve $I_T(K')$ is given in Figure 6.

The theoretical distribution, $I_T(K')$, must also be adjusted for the resolution of the system. The resolution of the system used in this experiment was 19% for the 392 kev peak of Sn^{113} and 30% for the 122+136 kev peak of Co^{57}. This correction is applied by considering each ordinate $I_T(K')$ as a discrete gamma ray which is recorded as a

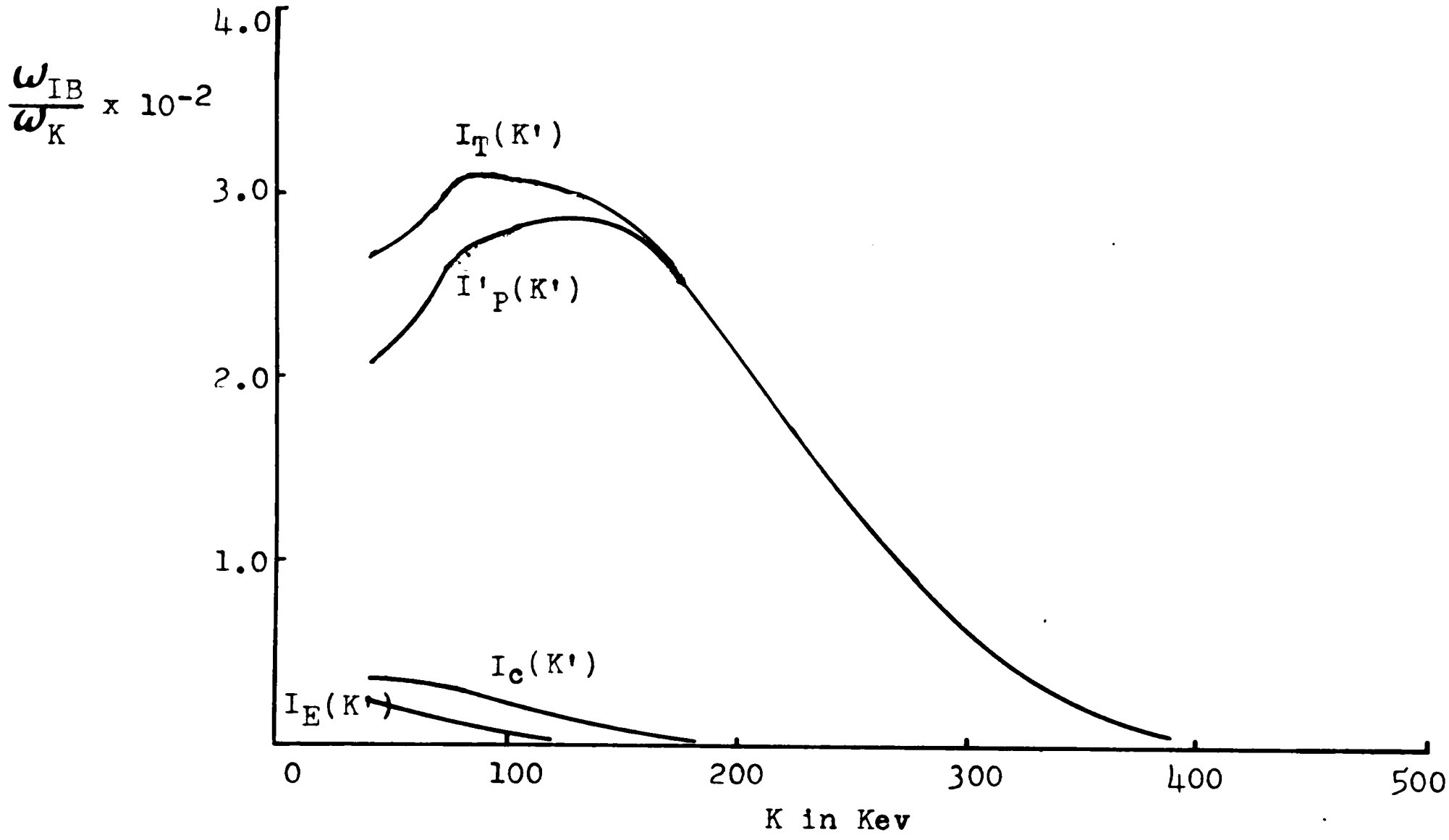

Figure 6. Theoretical IB Curve of Co^{57} Corrected for Crystal Effects

Gaussian distribution, g(K),

$$g(K) = \left[2\pi G\ K'\right]^{-\frac{1}{2}} \cdot \left[-\frac{(K'-K)^2}{2GK'}\right] .$$

The quantity G is given by

$$G = \frac{W^2(K')}{2K' \ln 2} ,$$

where W(K') is the half-width at half-intensity. The theoretical distribution corrected for resolution, $I_{RES}(K)$, is given by

$$I_{RES}(K) = \int_0^{K_{MAX}} I_T(K')\ g(K)\ dK' .$$

This correction is applied graphically and is outlined by Lindquist and Wu (9). A comparison of $I_{RES}(K')$ and $I_T(K')$ is given in Figure 7.

The corrections applied to the theoretical distribution due to crystal effects have been outlined in this section in the order of application. The theoretical distribution is now ready for a comparison with the experimental curve.

Analysis of the Experimental Data

Three runs, each with a duration of 70,000 seconds were made to obtain the true coincidence spectrum, the random coincidence spectrum, and the background coincidence spectrum. The gamma radiation from two sources was used for calibration,

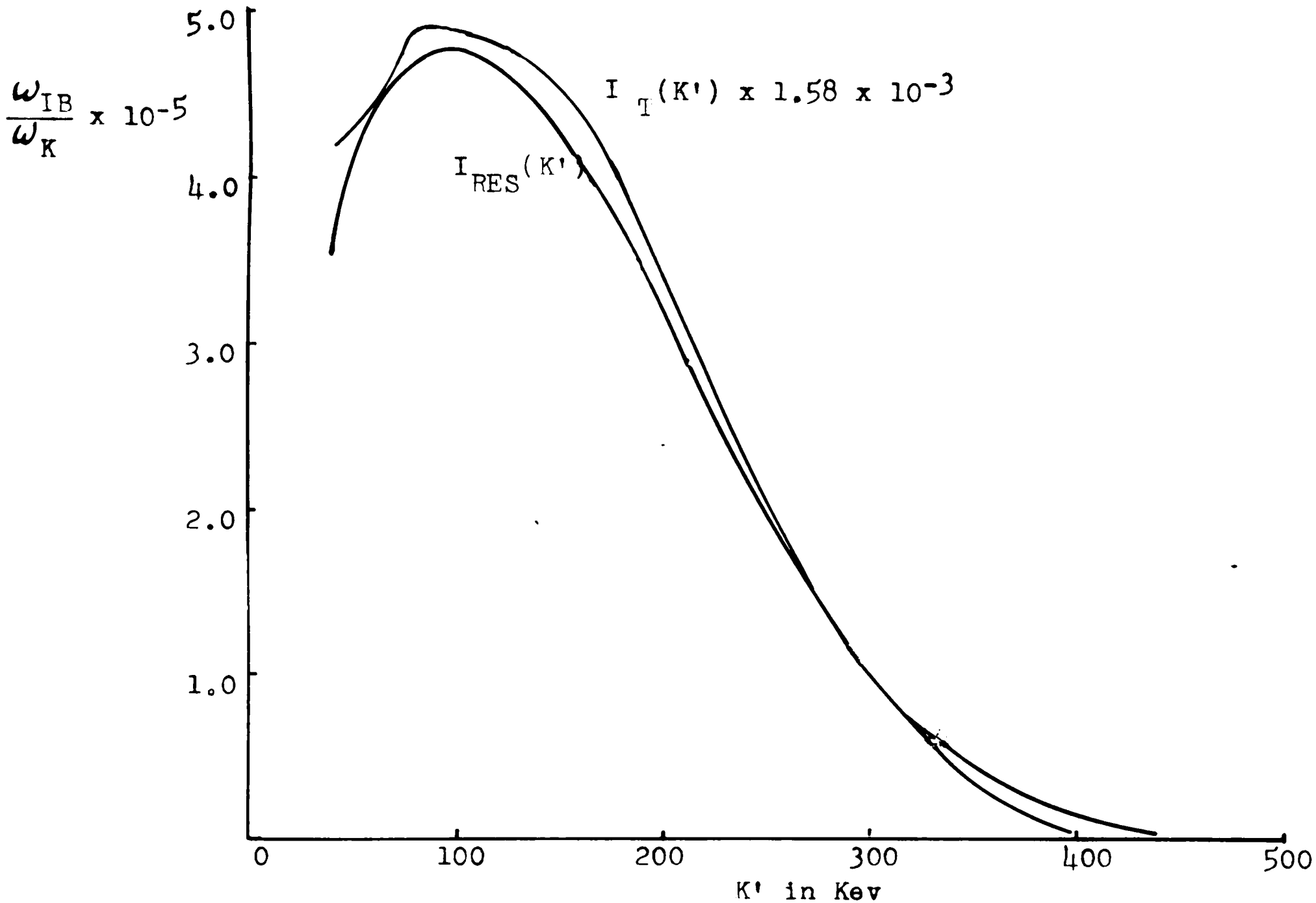

Figure 7. Comparison of Values for $I_I(K')$ and $I_{RES}(K')$

the 392 kev gamma ray of Sn^{113} and the 122 +136 kev peak of Co^{57}. The single channel count rate for the gated circuit was 1994 counts per second, and the single channel count rate for the ungated circuit was 3664 counts per second. The coincidence rate for these single channel count rates was 4.26 counts per second with a corresponding random rate of 3.62 counts per second. The background coincidence rate was 0.37 count per second. This gives a resolving time of 0.26×10^{-6} seconds for the system.

There are two ways in which the experimental curve can be compared with the corrected theoretical curve. The areas under the two curves may be compared as well as the distribution as a function of energy. The ratio of the total number of coincident counts which were indicated by the scaler to the total number of coincident counts which were recorded on the multichannel analyzer tape was 1.062 and the corresponding ratio for the random coincidences was 1.041. The difference in these two numbers is attributed to a small variation in the single channel count rates resulting from a drift in the amplifiers. By subtraction of the total number of random counts and the total number of background coincident counts from the total number of coincident counts above 70 kev, the total number of IB counts was found to be 13,083. If one used the values given above for the loss of coincident counts, the total number of IB counts above 70 kev was 19,973. This gives a

value of $7.35 \times 10^{-3} \pm 0.90 \times 10^{-3}$ for the area under the experimental curve. If the mean of the two values is used, the area under the experimental curve is $5.16 \times 10^{-3} \pm 0.90 \times 10^{-3}$. The corresponding area under the theoretical curve is 8.28×10^{-3}.

A comparison of the experimental distribution with the theoretical distribution is given in Figure 8. Because of the large concentration of random counts in the region of the 122 + 136 kev peak, the subtraction of the random spectrum from the coincidence spectrum is quite critical. A drift in the amplifier was evident because of the shift of the 122 + 136 kev peak of each spectrum. The scatter of the experimental distribution can probably be attributed to this drift.

If one assumes the validity of the Morrison and Schiff relation, a Fermi plot can be made to determine the disintegration energy. Letting $N = (\text{constant})\ K\ (1-K/W)^2$, one can plot $(N/K)^{1/2}$ versus K and obtain the endpoint of the IB spectrum. The Fermi plot is given in Figure 9. A least squares fit for the best straight line indicated an endpoint energy of 478 ± 30 kev. The disintegration energy is the binding energy of the K shell added to W; this gives a value of 484 ± 30 kev for the disintegration energy. This compares favorably with a previous value of 434 ± 30 kev obtained by Jung and Pool (10).

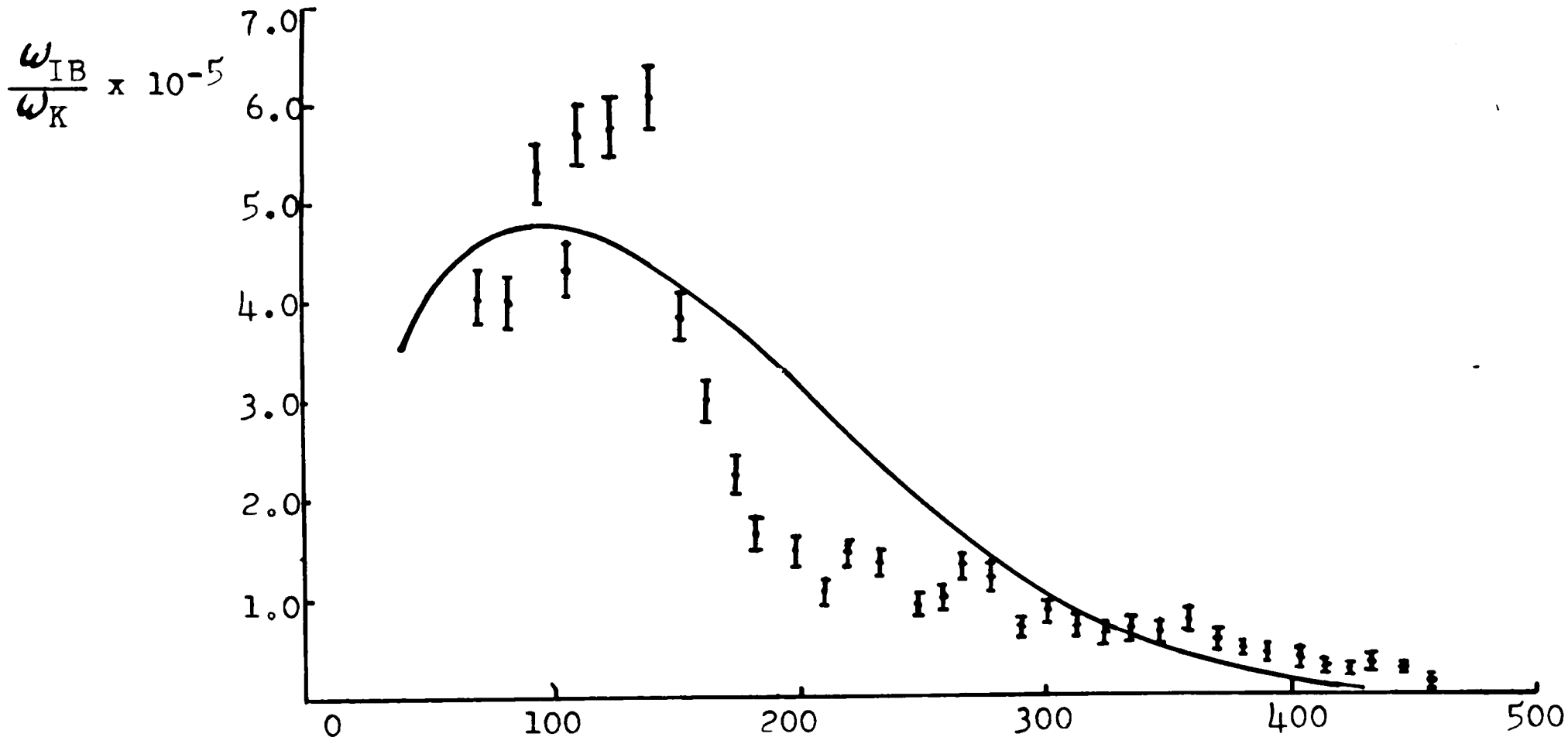

Figure 8. Comparison of Corrected Theoretical IB Curve of Co^{57} and Experimental Points

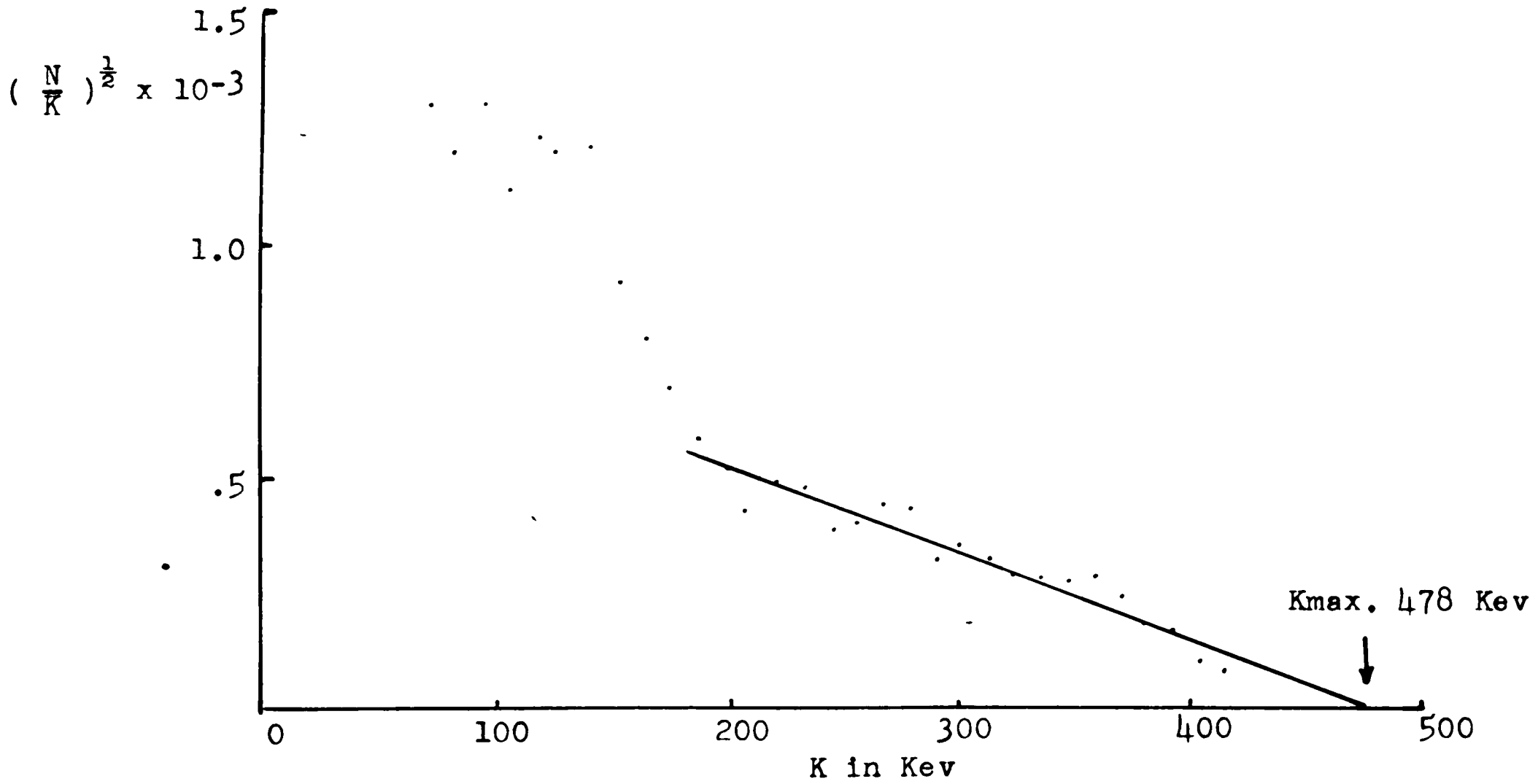

Figure 9. Fermi Plot of Co^{57} IB

CHAPTER V

CONCLUSION

The purpose of this thesis was to compare the absolute intensity of the inner Bremsstrahlung spectrum of Co^{57} as predicted by the Glauber and Martin theory with the experimentally observed spectrum. The general approach has been to correct the theoretical curve for crystal effects and then to compare the corrected theoretical curve with the experimentally observed spectrum. A comparison was made in two ways; by comparing the area under each curve above an energy of 70 kev and by comparing the distribution in energy of both curves. A correction for the variation in the single channel count rate was made on the coincident spectrum and on the random spectrum. Since the corrections on the two spectra were not the same, two different values for the area under the experimental curve were calculated; $7.35 \times 10^{-3} \pm 0.90 \times 10^{-3}$ from the mean of the two values. The area under the corrected theoretical curve was 8.28×10^{-3}.

While these values do not lie within the experimental error, they do indicate the possible validity of the Glauber and Martin theory. The relativistic correction, which is the most significant in this energy region, reduces the

prediction of Morrison and Schiff by about one-half. Since the area under the experimentally observed spectrum is less than that predicted by the Glauber and Martin theory, it would seem to indicate that the relativistic correction is of the right order of magnitude.

A comparison of the intensity as a function of energy reveals the experimental points are somewhat scattered. This is attributed to a drift in the amplifier during the experiment. A possible remedy for this drift is to superimpose two pulses of known energy upon the spectrum of each run so that the spectra may be accurately lined up when the processing of data starts.

A Fermi plot was made to determine the disintegration energy of Co^{57}. The value obtained was 484 ± 30 kev. A previously determined value by Jung and Pool (10) is 434 ± 30 kev.

LIST OF REFERENCES

1. Morrison, P., and Schiff, L. I., Physical Review 58, 24 (1940).

2. Glauber, R. J., and Martin, P. C., Physical Review 104, 158 (1956).

3. Glauber, R. J., and Martin, P. C., Physical Review 109, 1307 (1958).

4. Green, Alex E. S., Nuclear Physics (McGraw-Hill Book Co., Inc., New York, 1955), pp. 180-183.

5. Brysk, H., and Rose, M., Theoretical Results on Orbital Capture, Oak Ridge National Laboratory Report 1830 (unpublished, 1955).

6. Wapstra, A. H., Nijgh, C. J., and Lieshout, R. Van, Nuclear Spectroscopy Tables (Interscience Publishers, Inc., New York, 1959), p. 59.

7. Brenner, Abner, and Riddell, Grace, Journal of Research of the National Bureau of Standards 39, 385 (1947).

8. Heath, R. J., Scintillation Spectrometry Gamma Ray Spectrum Catalogue, Atomic Energy Commission Research and Development Report 11370 - 100.

9. Lindquist, T., and Wu, C. S., Physical Review 100, 145 (1955).

10. Jung, R. G., and Pool, M. L., Bulletin of the American Physical Society 1, No. 4, 172 E 11 (1956).